PCCP

ROYAL SOCIETY OF CHEMISTRY

REVIEW

View Article Online
View Journal | View Issue

Cite this: *Phys. Chem. Chem. Phys.*, 2025, **27**, 21387

Electrochemistry in conductive nanopipettes

Lan Lin,[a] Rujia Liu*[a] and Dengchao Wang *[ab]

Received 28th July 2025,
Accepted 8th September 2025

DOI: 10.1039/d5cp02868j

rsc.li/pccp

Conductive nanopipettes have been recognized as powerful tools for electrochemical measurements and imaging of various analytes of interest (*i.e.* ions, molecules, nanoparticles and cells), owing to their nanometer-sized tip, tuneable pipette geometry, and rich charge transport features. Meanwhile, the confined electroactive interface inside the nanopipette brings many new electrochemical behaviours which are quite different from their bulk counterpart. Studying these novel electrochemical processes in conductive nanopipettes not only reveals new physical insights into electrochemistry in confined spaces but also advances the emerging applications of nanopipettes for chemical analysis. This review summarizes the recent progress of conductive nanopipettes in terms of fabrication strategies, fundamental charge transport processes, and applications, highlighting their new electrochemical features and future prospects in analytical chemistry at the nanoscale.

Introduction

Benefiting from their nanometer-sized tip, hollow architecture, and versatile surface modification capabilities, nanopipettes have emerged as powerful tools in the realm of analytical chemistry over the past few decades.[1–3] In the early 20th century, Barber[4,5] started preparing pipettes with a tip diameter of 0.3–0.4 mm and used them to inject liquids and bacteria into living cells. This pioneering work laid the foundation for the development of modern nanopipette technology. In 1977, Brown and Flaming[6] first reported the fabrication of ultrafine microelectrodes with tip diameters as small as 20 nm. The advent of nanopipettes has provided a new tool for measurements in nanoscale research.

Nanopipettes are typically fabricated from quartz[7] or borosilicate[8] glass capillaries, which can be converted into two identical nanopipettes under sequential heating and pulling in a pipette puller. The geometry and size of nanopipettes can be characterized using transmission electron microscopy (TEM), scanning electron microscopy (SEM) and electrochemical methods.[9] A key strength of nanopipettes lies in their amenability to surface functionalization, allowing researchers to tailor the surface properties toward desired performances. Early modifications focused on altering the surface charge of nanopipettes using silanization or polymer coatings.[10] In recent years, the scope of nanopipette functionalization

[a] *School of Chemical Sciences, University of Chinese Academy of Sciences, Beijing 100049, P. R. China. E-mail: liurujia19@mails.ucas.ac.cn, wangdengchao@ucas.ac.cn*
[b] *Binzhou Institute of Technology, Weiqiao-UCAS Science and Technology Park, Binzhou 256606, Shandong Province, P. R. China*

Lan Lin

Lan Lin received her BS degree in Chemical Engineering from the Dalian University of Technology in 2017 and her MS degree in Chemical and Biomolecular Engineering from the Hong Kong University of Science and Technology in 2018. She is currently a PhD candidate at the University of Chinese Academy of Sciences. Her current research interests focus on electrochemical analysis based on conductive nanopipettes.

Rujia Liu

Rujia Liu obtained her BS degree in Chemical Engineering and Technology from Henan University in 2019. She then earned her PhD degree in Analytical Chemistry from the University of Chinese Academy of Sciences in 2024. Currently, she is a postdoctoral researcher at Beijing Normal University. Her research focuses on the development and application of electrochemical collision technology for single entities.

has expanded significantly. For example, conductive materials such as carbon[11] and gold[12] are now commonly used to coat nanopipettes, transforming them into electrochemical or photoelectrochemical platforms capable of multifunctional measurements that reveal fundamental ion transport, electron transfer, and optical properties of the systems.

Miniaturized pipettes with nanoscale dimensions also bring many new transport features that are quite different from their bulk counterpart. Owing to the excess surface charges or the electric double layer structure, confined inside the nanopipettes, many new transport phenomena such as ionic current rectification,[13] concentration polarization[14] and memory effects[15] have been reported and utilized in developing new sensing, separation and iontronic devices. Moreover, the incorporation of an electroactive interface into nanopipettes would bring new opportunities for monitoring and controlling both electron transfer and ion transport processes under the nanoscale confinements.[16] For example, very interesting bipolar electrochemical processes can occur at the two ends of the conductive layer when applying external bias between the inside and the outside electrodes,[11,17–20] while directly applying potentials at the conductive layer would lead to thin-layer electrochemical processes inside the pipettes.[21]

These rich and tuneable charge transport processes inside the conductive nanopipettes, including ion transport processes through the pipettes, the electron transfer processes at the conductive layer, and their interplays, also advance the practical applications for chemical analysis, especially at the single nanoparticle and single-cell level.[22–24] For example, the nanopipettes have been widely used to detect single nanoparticles *via* resistive pulse sensing methods,[25,26] with the size and surface charge information extracted from the blockage current transients.[27] Excitingly, the large electroactive interface inside the nanopipettes also allows the usage of electrochemical collision techniques for the detection and analysis of various types of nanoparticles, such as metal nanoparticles,[28,29] enzymes,[30] and liposomes.[31] Besides measuring single nanoparticles, the small sized tip would also allow the penetration of the pipettes through individual cells, enabling *in vivo* intracellular electrochemical measurements.[32] More importantly, with the merits of both nanopipettes and nanoelectrodes, many new operation modes have been proposed in conductive nanopipettes for single cell analysis, over classical amperometric tests at conventional disk nanoelectrodes. For example, the orifice diameter of a conductive nanopipette could be varied to match the size of the analytes for selective and sensitive detection. The additional conductive layer inside the pipette would also offer a new approach to control or regulate the mass transport processes, offering significant advantages for the qualitative and quantitative analyses of single entities and cells.

This article first introduces the fabrication and modification methods of nanopipettes, and then the fundamentals of the charge transport processes inside conductive nanopipettes are reviewed, including ion current rectification, thin-layer electrochemistry, bipolar electrochemistry, and ion transfer across the liquid–liquid interface. Finally, the applications of conductive nanopipettes in imaging, single entity analysis and single cell analysis are presented.

Dengchao Wang

Professor Dengchao Wang obtained his PhD degree in Chemistry from Georgia State University in 2015, under the supervision of Prof. Gangli Wang. Then, he worked as a postdoctoral fellow with Prof. Michael Mirkin at Queens College, City University of New York. In March 2019, he started the independent research at the University of Chinese Academy of Sciences and has been working on the fundamentals and applications of nanoelectroanalytical chemistry.

Fabrication

Glass nanopipettes

The nanopipettes are typically fabricated from a glass capillary based on either a pulling or a chemical etching method.[33] Nowadays, the laser heating and pulling method has become the most popular way to prepare nanopipettes owing to the easy and fast fabrication procedures. A laser puller could heat the middle part of the glass capillary and pull it into two nanopipettes with similar geometry and size. Obviously, the material (*i.e.* quartz and borosilicate) and size (*i.e.* inner and outer diameters) of the capillary would strongly affect the geometry and size of the resulting pipette.[34,35] In general, borosilicate glass is cheaper and suitable for fabricating nanopipettes with a relatively large size (*i.e.* diameter >80 nm) and a long needle length due to its soft nature with lower softening temperature. In comparison, quartz could be used to prepare both larger nanopipettes and ultra-small ones, with a lower noise level, better mechanical strength, chemical resistance and thermal stability under harsh conditions. In addition to the materials, the pipette geometry could also be fine-tuned by optimizing the pulling parameters such as heating temperature, pulling force and velocity.[35,36] For a nanopipette, the size at the orifice, the half-cone angle, as well as the glass wall thickness are the main geometry parameters, which can be characterized using TEM, SEM and electrochemical methods.[9]

To further extend the application of nanopipettes, a variety of physical and chemical modifications have been applied at the inner walls of the nanopipettes toward desired functions and properties. For example, analyte-recognition or stimuli-response elements can be physically or chemically modified at the inner walls to achieve high selective and sensitive detection.[9] Moreover, a carbon or metal layer was also introduced inside a pipette to offer an electrochemically or optically

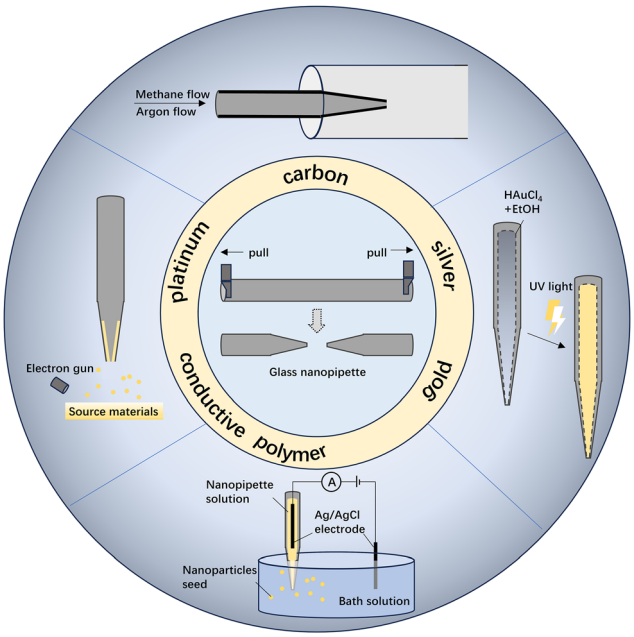

Fig. 1 Schematic diagram for fabricating conductive nanopipettes from glass nanopipettes.

active interface to enable powerful electrochemistry[37] or Raman analysis[38] inside the pipette. Therefore, various deposition methods have been proposed to develop conductive nanopipettes, and the conductive materials that can be deposited include carbon,[30] silver,[17] platinum,[18] gold[19] and conductive polymers,[10] as summarized in Fig. 1.

Chemical vapor deposition (CVD)

CVD is a commonly adopted technique to prepare carbon modified nanopipettes (CNPs). Bau *et al.*[39] and Gogotsi *et al.*[40] pioneered the early CVD method to deposit the carbon layer at the inner surface of the quartz pipette. Briefly, a carbon source (such as methane) and a protective gas (argon or nitrogen) are introduced into the nanopipette under heating in the range of 875–950 °C for approximately 0.5 to 1 hour. Notably, the gas flow rate and the length of the quartz capillary play crucial roles in the thickness of the carbon layer deposited inside the pipette, thus allowing for the customization of CNP tip geometries and diameters. Meanwhile, when increasing the deposition time, the resulting CNPs could gradually change from open pipettes to cavity electrodes,[21] and finally fully filled disk carbon nanoelectrodes.[41] The deposited carbon on the interior surface is characterized to be both amorphous and graphitic. As the carbon deposits on the whole interior surface of nanopipettes, the carbon layer can be easily connected to a potentiostat *via* a metal wire inserted inside the pipette.

The properties of the carbon can also be actively controlled toward desired chemical and electrochemical performances. Recently, we introduced gold nanoparticles (Au NPs) inside the glass pipettes as the catalysts to grow carbon nanotubes inside the CNPs.[42] The Au NPs are found to catalyse the methane decomposition processes at a lower temperature with faster deposition kinetics, and more importantly, carbon nanotubes (CNT) are clearly formed in the pipette orifice region, as observed from the TEM images. The prepared CNT modified carbon nanopipettes thus display a better electrochemical performance for glutathione and ascorbic acid, with a lower oxidation potential, higher current responses and smaller capacitive currents.

Electron-beam evaporation/magnetron sputtering

The physical vapor deposition (PVD) method, such as electron-beam evaporating and magnetron sputtering, is also a direct and simple way to coat the nanopipettes with a desired metal layer.[17] To get a uniform coating on the inner wall of the glass pipettes, the nanopipettes should be positioned vertically above the metal source. After deposition, the nanopipettes are immersed in HCl solution under a nitrogen gas stream to remove the metal layer on the exterior glass surface, and then the nanopipettes are washed and dried for use. In this case, the conductive layer cannot be directly connected to the potentiostat, and bipolar electrochemistry could be driven in the floating metal layer. Alternatively, a direct electric contact can be made to the deposited metal outside the pipette, which could be later covered with wax to leave a small region of the metal layer at the tip to serve as the electroactive interface. This method can be used to deposit metal layers such as silver,[17] platinum, and gold[19] inside the glass nanopipettes. Using such methods, an ~10 nm-thick metal layer can be deposited at the interior wall of the glass nanopipettes.

Chemical/photochemical deposition

The internal surface of the glass nanopipette can also be decorated with a thin metal layer *via* chemical or photochemical methods. For example, a gold film could slowly grow on the inner wall of glass nanopipettes from the filled $HAuCl_4$ and C_2H_5OH solution under UV irradiation. After successive washing, drying and annealing, an ultrathin gold-decorated nanopipette can be prepared with an estimated thickness of 2–4 nm.[12] Similarly, a gold film can also be *in situ* formed *via* a reaction between $HAuCl_4$ and H_2O_2.[43] The thickness of the prepared Au film is estimated to be around 2–5 nm from TEM characterization.

In addition, by loading metal salt (*i.e.* $HAuCl_4$ or H_2PtCl_6)[18,38] and reductant species (*i.e.* $NaBH_4$ or $NH_2OH{\cdot}HCl$)[20,38] inside or outside the nanopipette, respectively, the metal ions would be reduced into solid-state metals near the pipette pore region. Interestingly, such deposition processes could be actively controlled by applying bias voltages, as the mass transport through the nanopipette would control the overall reduction rate of the metal ions.[38]

In summary, the CVD method is mainly used for the deposition of carbon, which displays excellent electric conductivity and stability, and additional surface modification is needed to broaden its applications. The PVD method excels in producing various metal layers with high purities but requires post-etching or wax sealing of the metal layer outside

the pipette. The chemical or photochemical deposition methods are very simple and low cost, but the quality of the deposited metal layer is strongly affected by many factors (*i.e.* pipette geometry, surface properties and local ion concentration), which may not be easily and precisely controlled.

Fundamentals of conductive nanopipettes

For the conductive nanopipettes with both a pipette channel and a confined electroactive interface, many new operation setups and methods can be established toward desired measurements.[3] For example, the pipettes can be fully filled with the solution and two electrodes are put inside and outside the pipette, respectively, to measure the ionic current through the nanopipettes (Fig. 2a). Originating from the asymmetrical geometry and excess surface charges, very interesting and well-known non-linear ionic current rectification (ICR) can be observed in the resulting current–potential (*i*–*V*) curves. The nanopipettes are also an ideal platform to study the charge transfer reactions at liquid/liquid (L/L) interfaces owing to the miniaturized interface, enhanced mass transport, and potential applications as probes for the scanning probe microscopy techniques (Fig. 2b). Generally, the ion transfer at the L/L interface also produces Z-shaped *i*–*V* responses that could be fitted well to the Butler–Volmer equation. Interestingly, for the same experimental setup with two electrodes inside and outside the pipette, the bipolar electrochemical processes could occur at the two ends of the conductive layer (Fig. 2c), contributing to the overall current responses. Specifically, for the nanopipettes with a blocked or closed channel, dominating bipolar electrochemical responses can be observed in the resulting *i*–*V* curves. Alternatively, external bias could also be directly applied at the conductive layer, with respect to the reference and counter electrodes outside the pipette in the solution, which acts as a working electrode that measures the electron transfer processes at the conductive layer/solution interface (Fig. 2d). In this case, thin-layer electrochemical behaviour inside the cavity can be observed from the *i*–*V* curves, on top of the steady-state diffusion-controlled responses of the redox mediators from the bulk solution toward the pipette tip.

Ion current rectification

Ion current rectification (ICR) is one of the most well-known transport phenomena inside the nanopipettes. In general, the resistance of a nanopipette is a combination of the inside resistance and the excess resistance:[26]

$$R_p = R_{inside} + R_{access} \approx \frac{1}{\kappa\pi r \tan\beta} + \frac{1}{4\kappa r} \quad (1)$$

where r is the pipette radius at the orifice, κ is the solution conductivity, and β is the half-cone angle. Then, this equation can be used to estimate the size and the half-cone angle of the pipettes. The ionic resistance of a glass nanopipette is theoretically a constant value, so that a linear *i*–*V* response is expected. However, very interesting non-linear *i*–*V* responses are also observed in the nanopipettes, especially for those with a small tip size and at a low electrolyte concentration.[13] In 1997, Wei *et al.*[13] first reported the ICR phenomenon in conical nanopipettes under low electrolyte concentrations. The nanopipettes with tip radii ranging from 20 nm to 20 μm exhibited nonlinear current–voltage (*i*–*V*) characteristics in KCl solutions ($c < 0.1$ M). This asymmetry was attributed to the formation of an electrical double layer (EDL) at the quartz/electrolyte interface, which induces perm-selectivity and asymmetric ion transport through the nanopipette.

The ICR in glass nanopores/nanopipettes has already been well reviewed previously.[9,44] After modifying the conductive layer inside the pipettes, the ICR could become either larger or smaller, depending on the changes in the excess surface charge densities at the conductive layers. More interestingly, the double layer structure at the conductive layer/solution interface can now be actively controlled by an applied external bias. In a carbon nanopipette, the rectification was shown to increase greatly with increasing negative carbon bias, while at positive potentials, the rectification disappeared completely into a linear *i*–*V* response.[11] A similar trend is observed in the polyaniline modified nanopipettes, where the resulting current rectification could be actively and reversibly controlled by the switching potentials.[45] Besides directly applying potential at the conductive layer to tune surface charges and the EDL structure, the redox mediator in the solution could also be utilized to regulate the potential of the floating conductive layer and the resulting ICR.[46] The redox mediator with positive

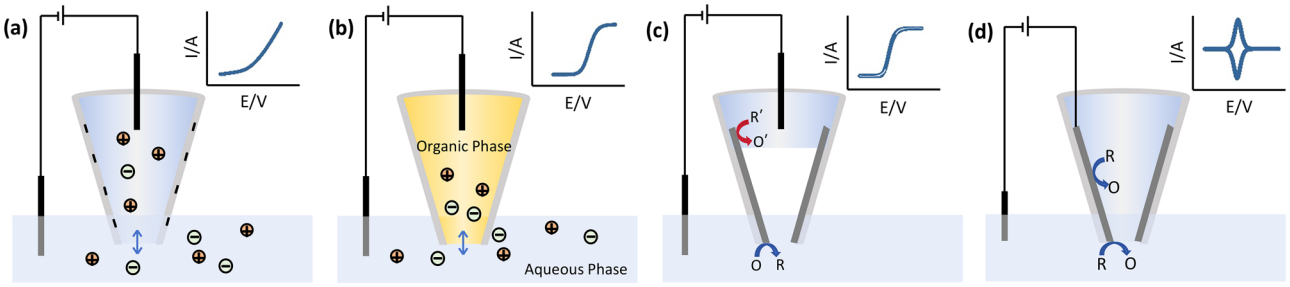

Fig. 2 Schematic representation of (a) ion current rectification (ICR), (b) electrochemistry through the liquid/liquid interface, (c) bipolar electrochemistry and (d) thin-layer electrochemistry in the nanopipettes.

formal potentials tends to decrease the negative charge density and the degree of ICR, while the redox mediator with negative formal potentials would increase the degree of ICR. As the ICR is very sensitive to the surface charges, such strategies could be further developed for the ICR sensing of redox species with extremely low concentrations (*i.e.* nM or pM).

Electrochemistry at liquid/liquid interfaces

Besides using the same solution inside and outside the pipette to investigate the mass transport processes, another interesting transport system is the charge transfer at a liquid/liquid (L/L) interface, or at an interface between two immiscible electrolyte solutions (ITIES). The very first study of electrochemistry at the L/L interface could be traced back to as early as 1902, when Nernst and others[47] found the current at the water/phenol/water interface when studying the transference numbers of coloured inorganic electrolytes in non-aqueous solvents. In 1986, Taylor and Girault[48] began to study the L/L interface on micropipettes, which showed many advantages in the minimization of the capacitive charging/discharging current and IR drop and a significantly increased mass transport rate. In recent years, Shao *et al.*[49–51] made many important explorations in the research of fundamentals and applications of L/L interfaces inside the nanoelectrodes and nanopipettes.

As two liquid phases are introduced inside the pipettes, many charge transfer reactions can thus be studied by the electrochemical methods in the nanopipettes, including the ion transfer reaction and the electron transfer reaction. When an ion transfers between the aqueous and oil phases, its valence state does not change, while only the solvation state changes, and this is a simple ion transfer reaction. Such a process could be a spontaneous process or facilitated by adding certain ionophores to complex with the transferred ion to reduce the overall transfer energy. As there is no change in the valence state of the ions during the ion transfer processes, the Nernst equation can be directly used to describe the ion transfer reaction at equilibrium, and similar sigmodal current responses can be obtained from the *i–V* curves, analogous to the electron transfer processes at the solid nanoelectrodes.[51] The diffusion limiting current from the ion transfer at the L/L interface thus has a similar form:[52]

$$i_{\mathrm{ing}} = 4xzFDca \qquad (2)$$

where F is the Faraday constant, c, D and z are the concentration, diffusion coefficient, and charges of the transferred ions, respectively, and x is the function of the RG value (radius of the pipettes/radius of the opening). Therefore, such an equation could also be used to measure the radius (a) of the pipette opening. It is worth pointing out that, compared to eqn (1), this equation could eliminate the effect from the half-cone angle, as the current is mainly from the ion transfer across the liquid–liquid interface.

Compared with ion transfer reactions, studying electron transfer reactions at the liquid/liquid interface is much more difficult, so that there are few systems that can be studied. The electron transfer reaction at the liquid/liquid interface can be studied only if two conditions are met: the potentials of the redox couples in the two phases (aqueous phase and organic phase) are matched, and both the reactants and products in the organic phase are insoluble in water and do not pass through the interface in the form of ion transfer.

Bipolar electrochemistry

The exactly same experimental setup used for the mass transport studies in nanopipettes could reveal additional interesting charge transport processes: bipolar electrochemical (BPE) processes could occur at the two ends of the conductive layer. As the applied voltage in the nanopipette is known to mainly drop near the pipette region within about several micrometers, the typical applied voltages of −1 to 1 V would be sufficient to drive the two redox reactions at the two ends of the conductive nanopipettes.[18,23] Such new bipolar electrochemistry inside the confined nanopipettes brings many new opportunities for the electrochemical sensing applications at the nanoscale.

The bipolar electrochemistry in nanopipettes can be classified into two configurations, an open and a closed channel.[19] In the closed configuration,[11] the inner solution is separated from the outer solution so that there is no actual ion transport process across the pipette. Such closed bipolar processes can be observed from the nanopipettes that are completely blocked by the deposited metals in the pore orifice region, or the solution is discontinued inside the pipette (Fig. 3a). Then, two reactions occur at the two ends of the conductive substrate, and all the current must flow through the floating conductive substrate. In this case, the closed BPE in the nanopipette actually acts as a disk electrode.

For the open bipolar electrochemical processes,[46] the current would flow through two parallel pathways: the ionic current through the pipette orifice and the electronic current through the conductive layer (Fig. 3b). The resulting current would thus include both the ionic current through the nanopipette and the electronic current through the conductive layer. In carbon deposited nanopipettes, one would gradually see that the overall current responses change from the typical rectified ionic current to the sigmodal-shaped electrochemical currents,[11] by increasing the redox mediator concentration from nM to mM. One signature of the bipolar electrochemical processes in the nanopipettes is $E_{1/2}$ = 0 V, regardless of the different formal potentials of different redox mediators.[46] This is because the floating conductive layer would reach an equilibrium with the solution potential established by the redox mediators, and external bias voltage between the two driving electrodes would drive the electron transfer processes at the carbon layer, leading to the sigmodal current responses. Following such a scenario, adding a certain redox mediator inside the conductive nanopipettes could regulate the potential of the floating conductive layer and the resulting ionic current.[52]

The beauty of the bipolar electrochemistry lies in the coupled two electron transfer processes at the two ends of the conductive substrate. Thus, the electrochemical reaction of interest could be revealed by the coupled reactions, which

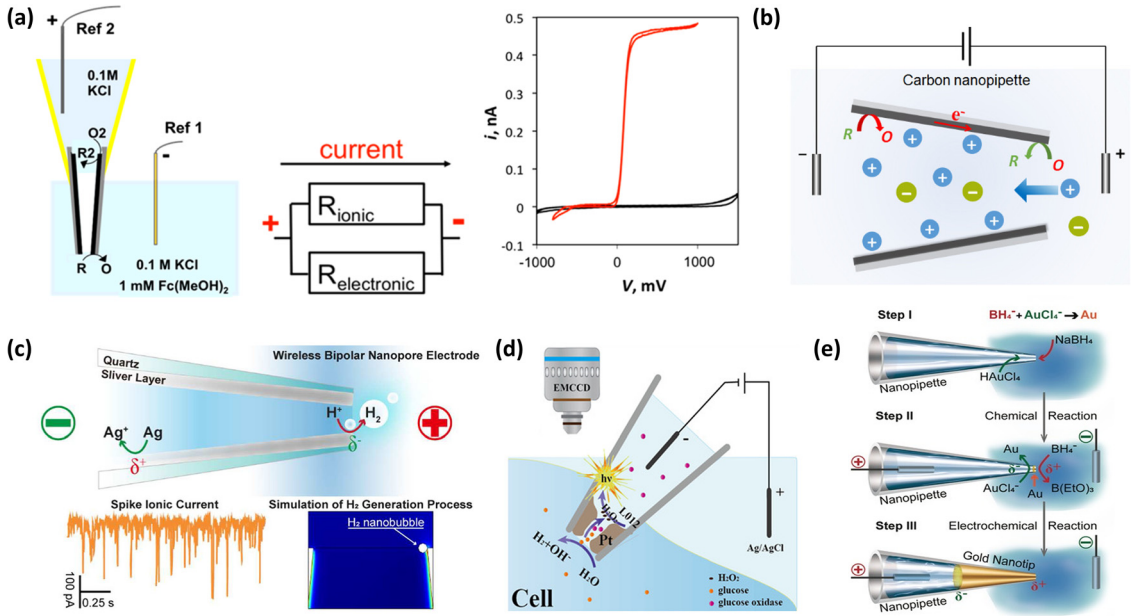

Fig. 3 The bipolar electrochemistry inside the conductive nanopipettes.

could be well designed to facilitate the quantification and visualization of the reactions. For example, Long *et al.*[17] developed a wireless bipolar nanopore electrode (WNE) coated with a silver layer to achieve ultrasensitive detection of single small molecules and ions (Fig. 3c). By leveraging bipolar electrochemistry, the WNE generates localized redox reactions at its ends, enabling the detection of H_2 (*via* H_2 nanobubbles), Ag^+ (*via* silver oxidation), and Hg^{2+} (*via* competitive reduction). This method offers a label-free alternative for real-time monitoring of electroactive species in complex environments. Jiang *et al.*[18] deposited porous Pt in the pipette orifice region to develop an open bipolar electrochemiluminescent (ECL) device to analyze the intracellular species (Fig. 3d). As the bias voltage mainly drops within the pipette tip, ECL could be generated at very low voltages below 100 V inside the pipette, which is about three orders of magnitude less than that in a classic bipolar setup. Then, the electrochemical reaction or the analytes of interest (*i.e.* H_2O_2 and glucose) inside the live cells can be visualized and quantified using the ECL signals.

In addition to the open bipolar setup inside the pipette, the pipette could also be fully blocked by the metal layer to form a closed bipolar configuration. Long *et al.*[20] used a rapid chemical–electrochemical fabrication method to produce a well-defined nanopore electrode with a size around 30 nm (Fig. 3e). Such a method could greatly simplify the conventional fabrication procedure for nanoelectrodes, which includes tedious and undisciplinable etching, sealing and polishing procedures. The prepared confined nanopore electrode could be used to measure the electrochemical processes *via* a bipolar approach and be potentially used for the surface enhanced Raman scattering detection. Moreover, the well-defined bipolar configuration and the small dimension of the nanopore would be ideal for the cellular detection with high sensitivity and spatial resolution.

Thin-layer electrochemistry

Besides studying the mass transport processes through nanopipettes, the conductive nanopipettes could also be directly used as working electrodes. By applying potential at the carbon layer, the conductive nanopipette could act as a nano-sampler, and typical thin-layer electrochemical responses with symmetrical oxidation/reduction peaks can be obtained in the resulting cyclic voltammograms. Meanwhile, the conductive layer at the pipette orifice which is exposed to the external solution would act as a nano-ring electrode to produce Z-shaped steady-state currents (curve 2 in Fig. 4b).[21] In this case, when used as an electrode, the conductive nanopipettes would produce a thin-layer electrochemical response on top of the Z-shaped steady-state currents (curve 1 in Fig. 4b). Interestingly, the peak currents would increase linearly with respect to the potential scan rate (Fig. 4c), while the steady-state current from the conductive ring at the orifice is largely scan-rate independent, and these two important features could be used to estimate the tip size and the cavity volume of the prepared conductive nanopipettes.

The size of the pipette could be estimated from the steady-state diffusion-limiting current (i_d), based on an equation that is similar to that used for the disk electrode:[53]

$$i_d = 4xnFDc^*r \quad (3)$$

where n, F, D, c^* and r are the number of transferred electrons, the Faraday constant, the diffusion coefficient, the redox mediator concentration in the bulk solution and the tip size, respectively. x is a dimensionless parameter that is related to the RG value of the pipette. A typical x value is $\sim$1.1 for conductive nanopipettes. Numerical simulations also show that 1 nm thickness carbon would account for at least 87% of the

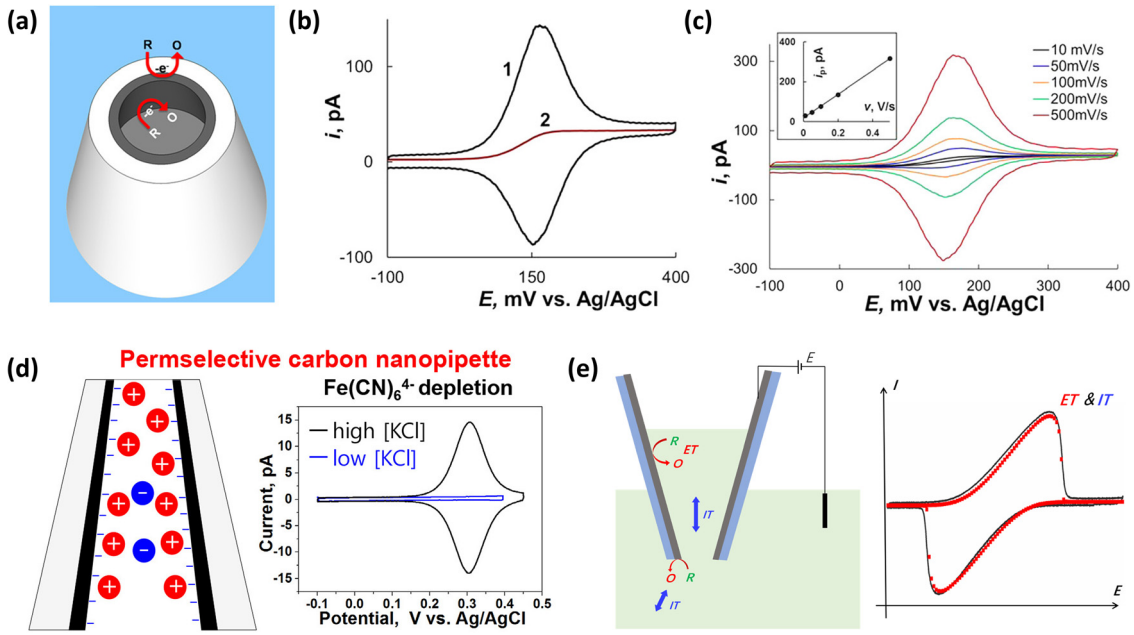

Fig. 4 Thin-layer electrochemistry inside the conductive nanopipettes.

steady-state current of the disk electrode with various sizes from 50 to 100 nm, and the half-cone angle of the pipette has no effect on the steady-state currents.[16] In this case, eqn (3) can be used to estimate the pipette size. On the other hand, the solution volume inside the pipette cavity can be estimated based on the integrated charges enclosed in the oxidation or reduction peaks, and a typical pL–aL solution volume is generally obtained for open carbon nanopipettes. To enable an accurate analysis, the contribution of the steady-state diffusion current as well as the double layer charging current needs to be subtracted first.[21] More importantly, a neutral redox mediator, such as FcMeOH, is desired for the solution volume evaluation, with a relatively high electrolyte concentration to minimize the electric double layer effect inside the nanopipettes.

The carbon surface is generally negatively charged due to the deprotonation of the surface carboxylic groups. Therefore, the carbon nanopipette could also have a confined EDL structure, which strongly affects the local concentration of the cations and anions, as well as the potential distribution normal to the carbon surface (Fig. 4d).[53] In the case of low electrolyte concentrations, redox cations would produce very small or even no current in the carbon nanopipettes, as they are largely excluded away from the cavity. On the other hand, much higher current could be obtained from redox cations. Such charge-selective electrochemical processes could be potentially used for selective detection of analytes carrying different charges. For example, negatively charged carbon nanopipettes would be able to differentiate dopamine, ascorbic acid and uric acid, based on either potential or the peak current, as they are positively charged, negatively charged and nearly neutral at selective pH.[54] Following a similar scenario, multivalent ions could adsorb onto negatively charged carbon surfaces,[55] effectively shielding surface charges, attracting more $Fe(CN)_6^{4-}$ ions inside the pipette, and thus enhancing the ET current responses.

In addition to the surface charge effect, the nano-confined small solution volume inside the pipette could also accelerate the chemical reactions. For example, two orders of magnitude increase in the enzymatic activity is reported for the conductive nanopipettes compared to the measured activity in the bulk solution.[56–58] Such an interesting confinement effect inside the nanopipette would offer an ideal model to study the enzyme-based catalytic reactions in a confined environment. The increased activity would also allow the direct experimental detection of single enzymes inside the conductive nanopipettes.[30]

As the thin-layer electrochemistry strongly depends on the solution volume inside the pipette, the external pressure was then used to actively control the solution volume and thin-layer electrochemical behaviour of the conductive nanopipettes.[59] As expected, the pressure could pump in and push out the inner solution from the pipette and lead to increased and decreased peak currents in the CVs. Meanwhile, the pressure would also polarize the concentration profile, and change the steady-state diffusion pattern, near the pipette orifice. Therefore, the steady-state current responses would also increase and decrease with respect to the external pressures. Compared to the closed disk- and fiber-shaped electrodes, the conductive nanopipettes with an open channel would facilitate the external pressure control of the solution volume and the resulting electrochemical behaviours, and the delivery and extraction of the measured solution of interest.

Ideal thin-layer electrochemical processes, with symmetrical oxidation/reduction peaks, can be observed in the conductive nanopipettes, when the solution volume is not large. For the conductive nanopipettes with a very deep solution depth,

the ion transport processes start to superimpose on the electrochemical processes. Our group[16] systematically investigated the charge transport processes within carbon nanopipettes (CNPs) through a combination of experimental and simulation approaches (Fig. 4e). With a simple coupled mass transport and electron transfer model, the experimental *i–V* responses under various conditions could be well fitted by the numerical simulation. Then, we examined the effects of the scan rate, the solution depth, the redox mediator concentration, and the electrolyte concentration on current signals. The results showed that ion transport dominated under conditions such as high scan rates, large solution depths, high redox mediator concentrations, or low electrolyte concentrations, while the electrochemical processes were predominant in the case of low potential scan rates, small solution depths and high electrolyte concentrations.

Numerical simulations

To help understand the complex charge transport processes in the conductive nanopipettes and quantitatively correlate the electrode parameters with the resulting current signals, numerical simulations are generally performed with the pre-defined pipette geometry and physical boundary conditions.

For a typical numerical simulation approach, a 2D/3D geometric model of a conductive nanopipette is first built, generally based on the TEM/SEM characterization. Then, the charge transport processes can be described by the equations. The mass transport process in the solution phase is typically described using the Nernst–Planck (NP) equation, including diffusion, migration, and convection terms:

$$J_i = -D_i\nabla c_i - \frac{z_i F}{RT}D_i\nabla c_i\nabla\varphi + uc_i \quad (4)$$

In eqn (4), J_i is the total flux of species, D_i is the diffusion coefficient of species, c_i is the volume concentration of species, z_i is the charge number of species, F is the Faraday constant, R is the universal gas constant, T is the absolute temperature, and φ is the solution-phase potential.

At the electrode/solution interface, the electrochemical reaction kinetics follow the Butler–Volmer (B–V) equation:

$$J_R = k^0 c_0 e^{-\alpha f(E-\varphi-E_0)} - k^0 c_R e^{(1-\alpha)f(E-\varphi-E_0)} \quad (5)$$

$$J_0 = -k^0 c_0 e^{-\alpha f(E-\varphi-E_0)} + k^0 c_R e^{(1-\alpha)f(E-\varphi-E_0)} \quad (6)$$

In eqn (5) and (6), J is the current density on the electrode surface, k^0 is the standard rate constant, E_0 is the standard potential of the reaction, E is the actual potential of the electrode, α is the charge transfer coefficient, $f = zF/RT$, and φ is the solution potential.

The electric potential distribution in the solution phase is described by the Poisson equation, which establishes a quantitative relationship between the potential gradient and volume charge density and is a key equation for analyzing the electric field-mass transport coupling effect:

$$\nabla^2(\varepsilon_0\varepsilon_r\varphi) = -F\sum_i z_i c_i \quad (7)$$

In eqn (7), ε_0 is the vacuum permittivity; the definitions of F, z_i, and c_i are consistent with those in eqn (4).

After coupling and solving the above equations, the total current of the electrode can be obtained by integrating the flux of redox species at the electrode/solution interface. Furthermore, with the aid of simulations, key information such as the potential distribution, current density distribution, and ion concentration distribution can be intuitively acquired, providing quantitative support for revealing the intrinsic mechanism of nanoscale electrochemical processes.

Applications

Imaging applications

One of the main applications of the nanopipettes is their use as tips in scanning probe electrochemical imaging applications, such as scanning ion conductance microscopy (SICM).[37,60,61] The tip can be brought close to the substrates of interest by monitoring the ion current change as a feedback signal. Then, the local ion concentration distribution at the substrate, which reveals either substrate topography or activity, can be imaged *via* constant-height scanning. In addition, taking advantage of the electrostatic interaction of the double layer of the pipettes and the charged substrates, different positive and negative feedback currents could be obtained when the tips are brought close to the substrate.[61] The resulting current responses can then be used for the surface charge mapping of various analytes, such as bacteria, living cells and lipid membranes. Recently, based on the intriguing non-zero cross point from the pinched hysteresis *i–V* curves in nanopipettes, we proposed a new method to directly image the surface potential distribution near the charged substrate.[61] The fundamentals and applications of SICM,[62] SECM[63] and SECCM[64] in the emerging fields of catalysis and biological fields have been comprehensively reviewed previously.

In addition to the bare glass nanopipettes, the addition of conductive layers into the nanopipettes would further promote their usage as new tips for scanning electrochemical microscopy. On the one hand, the conductive nanopipettes could be used as an SECM tip as the steady-state current is similar to that of a disk electrode. On the other hand, the transient current inside the pipette cavity could also be used as the reporting signal to monitor the tip–substrate distance.[37] Since the transient current is 4–5 orders of magnitude higher than the steady-state current, the developed transient SECM would display a much higher sensitivity compared to the conventional steady-state SECM technique. We have shown that the μM redox mediator or even pure capacitive charging/discharging current could produce noticeable feedback current to locate the tip position.[37] The proposed new SECM methods would achieve both high sensitivity and spatial resolution featuring the transient peak currents in the carbon nanopipettes and could find

great potential applications in biological and electrocatalytic studies.

Single nanoparticle detection

Nanomaterials have attracted extensive attention due to their widespread applications in various fields, including drug delivery,[65] catalysis,[66] environmental management[67] and energy conversion.[68] The properties of nanoparticles are significantly influenced by factors such as the size, the morphology, and surface attachment.[69] Traditional characterization methods for nanoparticles, including SEM[70] and TEM,[71] enable the investigation of the nanoparticle size, the morphology and the structure. However, these techniques cannot achieve real-time detection of single nanoparticles in solution, as they primarily characterize ensemble populations under vacuum conditions. Conventional electrochemical studies face analogous challenges: while multiple nanoparticles are typically detected simultaneously, the polydispersity and varying orientations of nanoparticles render the detection of individual nanoparticles challenging.[72] Therefore, developing *in situ* single-particle analysis and detection technologies to accurately establish structure–function relationships of single nanoparticles, as well as to identify their individual characteristics, is of great significance for the development of new nanomaterials and nanotechnology.

The electrochemical analysis of single nanoparticles, which can detect the properties such as surface charge and geometric size, has gradually come into focus. In 1970, DeBlois *et al.*[73] extended the Coulter method to achieve the detection of polystyrene nanoparticles by creating nanopores in irradiated polycarbonate plastic sheets. They elaborated on the principle of the resistive pulse technique, including voltage pulse generation from electrolyte displacement when particles pass through pores, and presented the relationships between resistive pulses and particle sizes. Since the 1990s, scientists have started to study the electrochemical behaviour of particles by investigating the interactions between particles and electrodes.

The electrochemical collision techniques or nanoimpact electrochemistry also provides a versatile and powerful method to reveal the physiochemical features of single nanoparticles.[28] Several different collision mechanisms have been proposed to investigate the nanoparticles with different properties, and the surface blockage strategy relies on the blocking of the faradaic current by the insulator nanoparticle on the electrode surface;[74] the catalytic amplification method is used to detect the nanoparticle when a catalytic reaction occurs at the nanoparticle once colliding on the inert electrode surface.[75] Electroactive nanoparticles can be directly detected by the oxidation and reduction of the colliding nanoparticles on the electrode.[76] A similar electrolysis system is the vesicles and micelles that contain redox content. Finally, for the dielectric materials with higher capacitance than the electrode, charging/discharging current from single analytes could also be obtained from the resulting *i*–*t* curves.[77] Obviously, the collision frequency of the analytes strongly depends on the electrode size so that the microelectrodes are generally used to conduct the electrochemical collision experiments.

The conductive nanopipettes, with both the pipette structure and the larger interior surface area, would thus be a perfect platform to conduct both resistive pulse and electrochemical collision experiments. Meanwhile, the confinement effect inside the nanopipette would also play a role in the collision results. Mirkin *et al.*[28] reported a single nanoparticle trapping technique using carbon nanopipettes to investigate the collision dynamics of iridium oxide (IrO_x) nanoparticles (Fig. 5a). By precisely controlling the solution volume within the nanopipette through pressure regulation, they isolated individual nanoparticles inside the pipette and observed characteristic current spikes corresponding to successive collision events. Through electrocatalytic amplifications of hydrogen peroxide oxidation combined with high-resolution TEM and simulations, they demonstrated that these nanoparticles exhibit elastic collision behaviour under nanoconfinement, attributed to synergistic effects between electrostatic repulsion and oxygen bubble-induced recoil forces. This work not only establishes a novel approach for single-particle electrochemical analysis but also provides fundamental insights into nanoconfined electrocatalysis and the design of nanoreactors.

When investigating the collision and electrolysis of single Ag nanoparticles inside the carbon nanopipettes, we observed both single and multiple spikes during the collision events of silver nanoparticles within carbon nanopipettes (Fig. 5b).[29] The measured collision frequency was higher than the theoretical diffusion-limited frequency, which indicates that the electrophoresis is the main driving force for the movement of particles. Interestingly, in the carbon nanopipettes, it is found that the electrochemically generated Ag^+ could not easily diffuse away from the cavity, as confirmed by the discrete reduction peaks when applying reverse negative potentials. The negative surface charges, together with the nanocavity, are believed to play an important role in the collision and electrolysis processes of single Ag NPs.

With the elucidated collision features inside the nanopipette, our group[30] utilized electrochemical collision strategies to investigate the electrocatalytic properties of single horseradish peroxidase (HRP) enzymes (Fig. 5c). When the HRP enzyme molecules land on the surface of the carbon nanopipette, a current drop occurs due to the blockage of $Fe(CN)_6^{4-}$ oxidation. Simultaneously, current transients are generated as the enzyme molecules catalyse the oxidation and reduction of H_2O_2.

With the conductive nanopipettes, Mirkin and colleagues[31] developed a new electrochemical resistive-pulse sensing methodology using carbon nanopipettes (CNPs) to achieve single liposome detection and content analysis (Fig. 5d). Unlike conventional resistive-pulse techniques (driven by electroosmosis and limited to single-biased ion current blockage), CNP-based sensing detects faradaic current transients from redox reactions at the conductive carbon surface as well, allowing signal acquisition under both positive and negative biases. Further experimentation demonstrated that redox-active species (*e.g.*, ferrocyanide) encapsulated in liposomes generated characteristic faradaic current spikes upon collision with the CNP lumen. Quantitative and qualitative assessments of liposomal

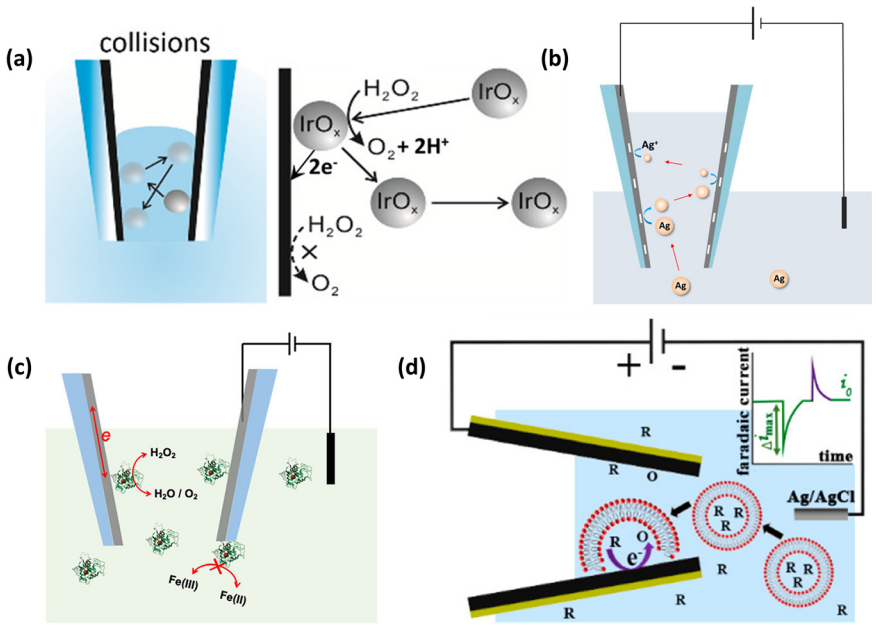

Fig. 5 (a) Experimental setup for monitoring collisions of a NP with a carbon nanopipette. Reproduced from ref. 28, with permission from American Chemical Society. (b) Electrochemical collision and oxidation of single AgNPs inside carbon nanopipettes. Reproduced from ref. 29, with permission from American Chemical Society. (c) Electrochemical collision of a single horseradish peroxidase enzyme inside the carbon nanopipette *via* catalytic amplification. Reproduced from ref. 30, with permission from American Chemical Society. (d) Resistive-pulse experiments involving translocation of liposomes through carbon nanopipettes. Reproduced from ref. 31, with permission from American Chemical Society.

vesicle payloads (*e.g.*, dopamine and nitrite) were accomplished through integrative analysis of these current transients. Such an electrochemical resistive pulse sensing technique could be very useful to analyse the liposomes or vesicles in practical applications, as the resistive pulse could be used to sort the appropriate-sized vesicles and evaluate their size based on the current drop, while the inner content could be calculated based on the integrated charges enclosed in the following electrolysis peaks. Then, these two pieces of information – the size and the number of molecules – could be accurately correlated, and the heterogeneity of the vesicles in size could be largely resolved.

Single cell analysis

Living cells contain diverse biomolecules, including bioactive substances within vesicles and lysosomes, where monitoring electron transfer, molecular dynamics and biochemical signalling molecules is critical to understand the complexities of life processes.[78,79] As the ionic current rectification (ICR) in the nanopipettes is very sensitive to the change in the surface charges and geometry, label-free ICR sensors have been developed for single living cell electrochemical analysis. A variety of analytes, including amino acids,[80] adenosine triphosphate (ATP),[81] K^+,[82] and reactive oxygen species,[83] have been analyzed based on the analyte-induced changes in ICR.

Alternatively, the disk nanoelectrodes could also be inserted in living cells to measure the intracellular species of interest. For example, Mirkin *et al.*[84] used platinum-coated CNPs integrated with SICM and SECM to achieve the quantification of relative abundances and dynamic variations of four reactive oxygen/nitrogen species (ROS/RNS) in living macrophage vesicles (Fig. 6a). These findings hold critical implications for *in situ* characterization of bioactive molecules in individual vesicles, with application potential for single-cell analysis and disease biomarker detection.

Moreover, the conductive nanopipettes, with the merits of both nanopipettes and nanoelectrodes, would allow multifunctional measurements with ion transport and electron transport processes.[79] The nanopipettes with a nanometer-sized tip and needle-like geometry can minimize the damage to the cells and allow *in vivo* electrochemical studies inside single living cells. With the fabricated powerful conductive nanopipettes and new charge transport features, various new emerging single cell electrochemical methods have been reported.

After depositing Pt inside the glass nanopipette, Pan and colleagues[85] developed a nanokit for single-cell electrochemical analysis of glucose levels and sphingomyelinase (SMase) activity (Fig. 6b). By integrating traditional assay components into a nanoscale capillary, the device used electrochemical pumping to release reagents into the cell, where glucose oxidase catalyzes H_2O_2 production or SMase-triggered sequential reactions generate H_2O_2. By analyzing the amount of H_2O_2 produced, they revealed heterogeneous intracellular glucose levels and unprecedented SMase activity dynamics. Later, Jiang and Pan *et al.*[86] designed an electrochemical molecular trap within a nanopipette to tackle the challenge of measuring low-abundance enzyme activity in an unstimulated cell (Fig. 6c). Electroosmotic flow (EOF) was employed to prevent molecules diffusing away from the electrochemical detector. Using this ultrasensitive electrochemical strategy, they measured the activity of 60 sphingomyelinase molecules in a single unstimulated live

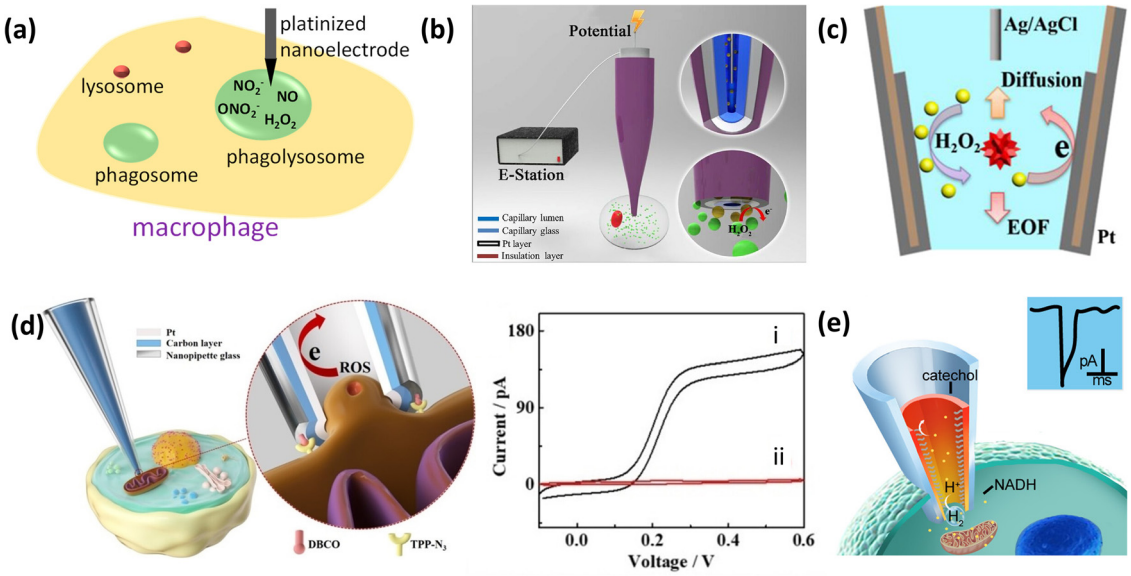

Fig. 6 (a) ROS/RNS analysis in living cells. Reproduced from ref. 84, with permission from American Chemical Society. (b) Schematic of the nanokit used for the single-cell electrochemical analysis. Reproduced from ref. 85, with permission from National Academy of Sciences. (c) The electroosmotic flow inside the conductive nanopipettes to help enrich the analytes of interest to allow the sensitive detection of low-abundance proteins. Reproduced from ref. 86, with permission from American Chemical Society. (d) Electrochemical setup for the capture and dynamic measurement of ROS released from one mitochondrion in a living MCF-7 cell. Voltammograms of FcMeOH with the nanopipette before (i) and after (ii) capturing one mitochondrion inside the living cell. Reproduced from ref. 87, with permission from Wiley. (e) The asymmetric nanopore electrode for single-cell probing. Reproduced from ref. 78, with permission from American Chemical Society.

J774 cell. Recently, Pan *et al.*[87] modified the tip of a nanocapillary electrode with dibenzocyclooctyl (DBCO). By leveraging the rapid click chemistry between DBCO groups at the tip and azide-substituted triphenylphosphine (TPP-N3) enriched in mitochondria, they captured single target mitochondria at the pipette tip (Fig. 6d). This method creates an independent detection zone within living cells, isolating the electrochemical detector inside the capillary from the captured single mitochondrion to avoid cytosolic interference, enabling *in situ* dynamic monitoring of reactive oxygen species (ROS) in individual mitochondria.

Long *et al.*[78] modified a conductive gold nanopipette with 4-thiol-catechol to achieve single-NADH molecule detection in live cells at a sensitivity of 1 pM (Fig. 6e). Applying a negative potential triggers the electrochemical reaction: catechol oxidizes to *o*-benzoquinone at the anode, while protons reduce to hydrogen gas at the cathode, forming nanobubbles that increase the ionic current by accumulating negative charges at the nanopore tip. In the presence of NADH, *o*-benzoquinone catalyzes NADH oxidation, creating a redox cycle that amplifies the current response for sensitive detection. Treatment with Taxol, which reduces intracellular NADH, significantly decreased the current amplitude and frequency, demonstrating its application potential for single-cell studies of anticancer drug effects on redox metabolism.

Besides measuring the ions and molecules in the cells, the nanoparticles inside the cells could also be detected with the conductive nanopipettes. Taking advantage of the developed electrochemical resistive pulse technique, Mirkin *et al.*[88] investigated the vesicles released from single living cells using both experimental and simulation approaches. The results showed that the blockage current was mainly determined using the liposome/CNP radius, independent of the pipette geometry, surface charge, or the vesicle trajectory. Faradaic transient current spikes were influenced by factors such as the collision location within the nanopipette, the cargo release mechanism, and the mass transfer rate, while the total transferred charge depended on the amounts of redox species in single vesicles. This study established a robust theoretical framework for single-vesicle characterization.

Summary and outlook

In summary, this review has summarized the fundamental charge transport processes inside conductive nanopipettes and practical sensing and imaging applications exploiting such interesting electrochemical processes. In general, the incorporation of a conductive layer inside nanopipettes would not only allow the direct measurements of electrochemical and optical processes but also bring new opportunities to tune and regulate the involved charge transport processes, such as ionic current rectification, bipolar electrochemistry and thin-layer electrochemistry. A variety of analytes, including redox molecules, ions, and nanoparticles, can be selectively and sensitively detected using the developed conductive nanopipettes. More importantly, the small-sized tip would further promote the usage of the conductive nanopipettes in high-resolution imaging applications and single cell analysis.

Despite significant progress in the fabrication and application of conductive nanopipettes, there remain some challenges

to be addressed. For example, the fabricated electrodes could still vary a lot between different batches in geometry and surface properties, which would strongly affect the reproducibility of the electrochemical tests. The additional surface modification of emerging new nanomaterials with unique physiochemical properties would improve their electrochemical performance, but the direct characterization of the surface functionalization would still be very difficult as they are confined deep inside the pipette. Meanwhile, the quantification of the reporting signals would also be difficult as many factors could contribute to the resulting current signals. Numerical simulations might be needed to help reveal the complicated charge transport processes inside the conductive nanopipettes. It is also worth pointing out that at this stage, most studies still focus on very simple and facile electrochemical processes and complex electron transfer processes, especially those coupled with chemical reactions are rarely investigated in the conductive nanopipettes. Studying the relatively complicated chemical and electrochemical reactions inside the confined nanopipettes would be of great fundamental importance as well as significant for the electrochemical tests in real biological samples and catalytic systems.

Conflicts of interest

There are no conflicts to declare.

Data availability

No primary research results, software or code have been included and no new data were generated or analyzed as part of this review.

Acknowledgements

The support of this work by the National Natural Science Foundation of China (22374150) and Fundamental Research Funds for the Central Universities is greatly appreciated.

References

1 X. Wang, J. Lv, X. Wu, Q. Hong and R. Qian, *ChemPlusChem*, 2023, **88**, e202300100.
2 S. Zheng, M. Wu, X. Wang, S. Xu and R. Qian, *ChemBioChem*, 2025, **26**, e202400879.
3 R. Yu, Y. Ying, R. Gao and Y. Long, *Angew. Chem., Int. Ed.*, 2018, **58**, 3706–3714.
4 M. A. Barber, *J. Kans. Med. Soc.*, 1904, **4**, 489–494.
5 M. A. Barber, *J. Infect. Dis.*, 1911, **8**, 348–360.
6 K. T. Brown and D. G. Flaming, *Neuroscience*, 1977, **2**, 813–827.
7 P. Pandey, A. Sesena-Rubfiaro, S. Khatri and J. He, *Faraday Discuss.*, 2022, **233**, 315–335.
8 M. Demirtas, *Brain Behav.*, 2024, **14**, e3405.
9 Y. Wang, D. Wang and M. V. Mirkin, *Proc. R. Soc. A*, 2017, **473**, 20160931.
10 S. Liu, Y. Dong, W. Zhao, X. Xie, T. Ji, X. Yin, Y. Liu, Z. Liang, D. Momotenko, D. Liang, H. H. Girault and Y. Shao, *Anal. Chem.*, 2012, **84**, 5565–5573.
11 K. Hu, Y. Wang, H. Cai, M. V. Mirkin, Y. Gao, G. Friedman and Y. Gogotsi, *Anal. Chem.*, 2014, **86**, 8897–8901.
12 X. Xu, H. He and Y. Jin, *Anal. Chem.*, 2015, **87**, 3216–3221.
13 C. Wei and A. J. Bard, *Anal. Chem.*, 1997, **69**, 4627–4633.
14 W. Shi, N. Sa, R. Thakar and L. A. Baker, *Analyst*, 2012, **140**, 4835–4842.
15 D. Wang, W. Brown, Y. Li, M. Kvetny, J. Liu and G. Wang, *Anal. Chem.*, 2017, **89**, 11811–11817.
16 R. Liu, Y. Ma, X. Shen and D. Wang, *Chem. Sci.*, 2021, **12**, 14752–14757.
17 R. Gao, Y. Ying, Y. Hu, Y. Li and Y. Long, *Anal. Chem.*, 2017, **89**, 7382–7387.
18 Y. Wang, R. Jin, N. Sojic, D. Jiang and H. Y. Chen, *Angew. Chem., Int. Ed.*, 2020, **59**, 10416–10420.
19 R. Gao, Y. Lin, Y. Ying, Y. Hu, S. Xu, L. Ruan, R. Yu, Y. Li, H. Li, L. Cui and Y. Long, *Nat. Protoc.*, 2019, **14**, 2015–2035.
20 R. Gao, Y. Ying, Y. Li, Y. Hu, R. Yu, Y. Lin and Y. Long, *Angew. Chem., Int. Ed.*, 2017, **57**, 1011–1015.
21 Y. Yu, J. Noël, M. V. Mirkin, Y. Gao, O. Mashtalir, G. Friedman and Y. Gogotsi, *Anal. Chem.*, 2014, **86**, 3365–3372.
22 G. Bulbul, G. Chaves, J. Olivier, R. E. Ozel and N. Pourmand, *Cells*, 2018, **7**, 55.
23 W. Yi, X. Li, X. He, F. Yue and T. Wang, *J. Electroanal. Chem.*, 2022, **909**, 116106.
24 K. Kececi, A. Dinler and D. Kaya, *J. Electrochem. Soc.*, 2022, **169**, 027502.
25 D. Kaya, K. Kececi and D. Yilmaz, *J. Indian Chem. Soc.*, 2019, **96**, 1149–1154.
26 Y. Wang, K. Kececi, M. V. Mirkin, V. Mani, N. Sardesai and J. F. Rusling, *Chem. Sci.*, 2013, **4**, 655–663.
27 Y. Liu, C. Xu, T. Gao, X. Chen, J. Wang, P. Yu and L. Mao, *ACS Sens.*, 2020, **5**, 2351–2358.
28 M. Zhou, Y. Yu, K. Hu, H. L. Xin and M. V. Mirkin, *Anal. Chem.*, 2017, **89**, 2880–2885.
29 R. Liu, X. Shen and D. Wang, *Anal. Chem.*, 2021, **93**, 7394–7398.
30 X. Shen, R. Liu and D. Wang, *Anal. Chem.*, 2022, **94**, 8110–8114.
31 R. Pan, K. Hu, D. Jiang, U. Samuni and M. V. Mirkin, *J. Am. Chem. Soc.*, 2019, **141**, 19555–19559.
32 W. Guo, Y. Wang, G. Qi, J. Wang, J. Ren, Y. Jin and E. Wang, *Anal. Chim. Acta*, 2024, **1293**, 342200.
33 C. Gao, S. Ding, Q. Tan and L. Gu, *Anal. Chem.*, 2009, **81**, 80–86.
34 Y. Zhou, L. Sun, S. Watanabe and T. Ando, *Anal. Chem.*, 2021, **94**, 324–335.
35 J. Stanley and N. Pourmand, *APL Mater.*, 2020, **8**, 100902.
36 S. Zhang, M. Li, B. Su and Y. Shao, *Annu. Rev. Anal. Chem.*, 2018, **11**, 265–286.
37 Y. Ma, Y. Zhao, R. Liu and D. Wang, *Anal. Chem.*, 2022, **94**, 11124–11128.

38 H. Li, D. Yang, A. Liu, G. Liu, Y. Shan, G. Yang and J. He, *Chin. J. Anal. Chem.*, 2019, **47**, e19104–e19112.
39 M. G. Schrlau, E. M. Falls, B. L. Ziober and H. H. Bau, *Nanotechnology*, 2008, **19**, 015101.
40 R. Singhal, S. Bhattacharyya, Z. Orynbayeva, E. Vitol, G. Friedman and Y. Gogotsi, *Nanotechnology*, 2010, **21**, 015304.
41 T. Sun, D. Wang and M. V. Mirkin, *Faraday Discuss.*, 2018, **210**, 173–188.
42 Y. Wang, Y. Zhao, Y. Ma and D. Wang, *Anal. Chem.*, 2024, **96**, 19933–19938.
43 H. He, X. Xu and Y. Jin, *Anal. Chem.*, 2014, **86**, 4815–4821.
44 Y. Xu, Y. Ruan, T. Zhang, X. Shi, H. Wang, W. Zhao, H. Chen and J. Xu, *TrAC, Trends Anal. Chem.*, 2023, **167**, 117217.
45 G. Pérez-Mitta, W. A. Marmisollé, C. Trautmann, M. E. Toimil-Molares and O. Azzaroni, *J. Am. Chem. Soc.*, 2015, **137**, 15382–15385.
46 D. Wang and M. V. Mirkin, *J. Am. Chem. Soc.*, 2017, **139**, 11654–11657.
47 W. Nernst and E. H. Riesenfeld, *Ann. Phys.*, 2006, **313**, 600–608.
48 G. Taylor and H. H. Girault, *J. Electroanal. Chem.*, 1986, **208**, 179–183.
49 P. Jing, M. Zhang, H. Hu, X. Xu, Z. Liang, B. Li, L. Shen, S. Xie, C. M. Pereira and Y. Shao, *Angew. Chem., Int. Ed.*, 2006, **45**, 6861–6864.
50 Q. Li, S. Xie, Z. Liang, X. Meng, S. Liu, H. H. Girault and Y. Shao, *Angew. Chem., Int. Ed.*, 2009, **48**, 8010–8013.
51 P. He, Y. Shao, Z. Yu, X. Liang, J. Liu, Y. Bian, Z. Zhu, M. Li, C. M. Pereira and Y. Shao, *Anal. Chem.*, 2022, **94**, 9801–9810.
52 C. B. Milton, K. Xu and M. Shen, *Curr. Opin. Electrochem.*, 2022, **34**, 101005.
53 J. H. Bae, D. Wang, K. Hu and M. V. Mirkin, *Anal. Chem.*, 2019, **91**, 5530–5536.
54 C. Yang, K. Hu, D. Wang, Y. Zubi, S. T. Lee, P. Puthongkham, M. V. Mirkin and B. J. Venton, *Anal. Chem.*, 2019, **91**, 4618–4624.
55 Y. Wang, R. Liu, X. Shen and D. Wang, *J. Phys. Chem. Lett.*, 2022, **13**, 11369–11374.
56 K. J. Vannoy, A. Ryabykh, A. I. Chapoval and J. E. Dick, *Analyst*, 2021, **146**, 3413–3421.
57 Y. Zhang, J. Ge and Z. Liu, *ACS Catal.*, 2015, **5**, 4503–4513.
58 H. He, X. Xu, H. Wu, Y. Zhai and Y. Jin, *Anal. Chem.*, 2013, **85**, 4546–4553.
59 R. Liu and D. Wang, *ACS Sens.*, 2022, **7**, 1138–1144.
60 R. Pan, K. Hu, R. Jia, S. A. Rotenberg, D. Jiang and M. V. Mirkin, *J. Am. Chem. Soc.*, 2020, **142**, 5778–5784.
61 Y. Ma and D. Wang, *Anal. Chem.*, 2021, **93**, 15821–15825.
62 C. Zhu, K. Huang, N. P. Siepser and L. A. Baker, *Chem. Rev.*, 2020, **121**, 11726–11768.
63 D. Polcari, P. Dauphin-Ducharme and J. Mauzeroll, *Chem. Rev.*, 2016, **116**, 13234–13278.
64 C. L. Bentley, J. Edmondson, G. N. Meloni, D. Perry, V. Shkirskiy and P. R. Unwin, *Anal. Chem.*, 2018, **91**, 84–108.
65 C. Zhang, A. Hemmat, N. H. Thi and M. Afrand, *J. Mol. Liq.*, 2025, **424**, 126999.
66 P. Lakhani, D. Bhanderi and C. K. Modi, *J. Nanopart. Res.*, 2024, **26**, 148.
67 W. Zhu, Y. Yue, H. Wang, B. Zhang, R. Hou, J. Xiao, X. Huang, A. Ishag and Y. Sun, *J. Environ. Chem. Eng.*, 2023, **11**, 110164.
68 J. Zeng, Y. Xuan and Q. Li, *Energy*, 2023, **280**, 128187.
69 M. Namakka, M. R. Rahman, K. A. M. B. Said, M. Abdul Mannan and A. M. Patwary, *Environ. Nanotechnol., Monit. Manage.*, 2023, **20**, 100900.
70 M. Lal, P. Sharma and C. Ram, *Optik*, 2021, **241**, 166934.
71 R. W. Lodge, W. J. Cull, A. Weilhard, S. P. Argent, J. Alves Fernandes and A. N. Khlobystov, *Nanoscale*, 2025, **17**, 10105–10116.
72 M. V. Mirkin, T. Sun, Y. Yu and M. Zhou, *Acc. Chem. Res.*, 2016, **49**, 2328–2335.
73 R. W. DeBlois and C. P. Bean, *Rev. Sci. Instrum.*, 1970, **41**, 909–916.
74 B. Quinn, P. G. Van't hof and S. Lemay, *J. Am. Chem. Soc.*, 2004, **126**, 8360–8361.
75 X. Xiao and A. Bard, *J. Am. Chem. Soc.*, 2007, **129**, 9610–9612.
76 Y. Zhou, N. V. Rees and R. G. Compton, *Angew. Chem., Int. Ed.*, 2011, **50**, 4219–4221.
77 J. Poon, C. Batchelor-McAuley, K. Tschulik and R. G. Compton, *Chem. Sci.*, 2015, **6**, 2869–2876.
78 Y. Ying, Y. Hu, R. Gao, R. Yu, Z. Gu, L. P. Lee and Y. Long, *J. Am. Chem. Soc.*, 2018, **140**, 5385–5392.
79 R. Jia and M. V. Mirkin, *Chem. Sci.*, 2020, **11**, 9056–9066.
80 Y. Xu, Y. Ruan, H. Wang, S. Yu, X. Yu, W. Zhao, H. Chen and J. Xu, *Small*, 2021, **17**, 2100503.
81 K. Zhang, T. Xiong, F. Wu, Q. Yue, W. Ji, P. Yu and L. Mao, *Sci. China: Chem.*, 2020, **63**, 1004–1011.
82 X. Shi, Y. Ruan, H. Wang, W. Zhao, J. Xu and H. Chen, *CCS Chem.*, 2021, **3**, 2359–2367.
83 J. Song, C. Xu, S. Huang, W. Lei, Y. Ruan, H. Lu, W. Zhao, J. Xu and H. Chen, *Angew. Chem., Int. Ed.*, 2018, **57**, 13226–13230.
84 K. Hu, Y. Li, S. A. Rotenberg, C. Amatore and M. V. Mirkin, *J. Am. Chem. Soc.*, 2019, **141**, 4564–4568.
85 R. Pan, M. Xu, D. Jiang, J. D. Burgess and H. Chen, *Proc. Natl. Acad. Sci. U. S. A.*, 2016, **113**, 11436–11440.
86 R. Pan, D. Wang, K. Liu, H. Chen and D. Jiang, *J. Am. Chem. Soc.*, 2022, **144**, 17558–17566.
87 K. Liu, Z. Zhang, R. Liu, J. Li, D. Jiang and R. Pan, *Angew. Chem., Int. Ed.*, 2023, **62**, e202303053.
88 R. Liu, R. Jia, D. Wang and M. V. Mirkin, *Anal. Chem.*, 2023, **95**, 13756–13761.